Synthesis of polyoxometalate encapsulated in uio-66(zr) with hierarchical porosity and double active sites for oxidation desulfurization of fuel oil at room temperature

Gan Ye, Yulong Gu, Christine Lancelot, Alain Rives, Carole Lamonier, Nicolas Nuns, Maya Marinova, Wei Xu, Yinyong Sun

Synthesis of polyoxometalate encapsulated in UiO-66(Zr) with hierarchical porosity and double active sites for oxidation desulfurization of fuel oil at room temperature

Gan Ye[a], Yulong Gu[a], Christine Lancelot[b], Alain Rives[b], Carole Lamonier[b], Nicolas Nuns[c], Maya Marinova[c], Wei Xu[d], Yinyong Sun[a,*]

[a]*MIIT Key Laboratory of Critical Materials Technology for New Energy Conversion and Storage, School of Chemistry and Chemical Engineering, Harbin Institute of Technology, Harbin, 150001, China*

[b]*Univ. Lille, CNRS, Centrale Lille, ENSCL, Univ. Artois, UMR 8181 - UCCS - Unité de Catalyse et Chimie du Solide, F-59000 Lille, France*

[c]*Institut Chevreul, University of Lille & CNRS, Villeneuve d'Ascq F-59655, France*

[d]*State Key Lab of Inorganic Synthesis and Preparative Chemistry, College of Chemistry, Jilin University, Changchun, 130012, China*

*To whom correspondence should be addressed.

Tel: 86 451 86413708

E-mail: yysun@hit.edu.cn

Abstract: Catalytic oxidative desulfurization (ODS) of fuel oil has received much attention. For this, the development of highly efficient ODS catalyst is of practical importance. In this work, we report that new ODS catalyst consisting of $H_3PW_{12}O_{40}$ (PW) and UiO-66(Zr) was developed without the addition of any solvent. As a result, the catalyst exhibited extraordinary catalytic activity by using H_2O_2 as oxidant in the ODS reactions of benzothiophene, dibenzothiophene and 4,6-dimethyldibenzothiophene. The TOF number for the removal of DBT reached 221.4 h^{-1} at room temperature, which is much higher than that of the reported catalysts. Such outstanding catalytic performance could be mainly attributed to easy accessibility of active sites and the existence of two types of active centers from PW species and defective UiO-66(Zr).

1. Introduction

With the increasingly stringent regulations, desulfurization of fuel oil is of great importance for producing clean energy[1-6]. However, it is difficult to remove the sulfur-containing molecules like 4,6-dimethyldibenzothiophene (4,6-DMDBT) in fuel oil due to the steric hindrance effect from alky-groups on the aromatic rings by industrial hydrodesulfurization (HDS) process[7-10]. Oxidative desulfurization (ODS) is regarded as one of the most promising processes to remove these aromatic sulfur-containing compounds due to its favorable features such as no hydrogen consumption and low cost of operation[11-14]. Thus, many research works have been focused on the development of ODS catalysts with high desulfurization efficiency[15-17]. Although some works about the preparation of novel ODS catalysts have been done, it is still rare that the catalysts can exhibit highly efficient ODS ability at room temperature and ambient pressure.

Polyoxometalates (POMs), as typical metal oxide cluster anions, have displayed great potentials in many applications[18-21]. However, due to their low surface area and easy solubility in solvent, it is difficult to utilize POMs as heterogeneous catalysts[22-24]. To overcome this difficulty, many works were focused on POMs supported or encapsulated in porous materials [25-28]. As a result, the composite materials prepared by these methods can display heterogeneous character to some extent. However, the loss of POMs in these materials would still occur during the reactions[29,30]. Additionally, the accessibility of active centers could be poor due to the block of pore channels resulting from the introduction of PW species. For this, preparing a highly efficient heterogeneous catalyst with easy accessibility of POMs active sites maintains a great challenge.

In this work, we report that new composite materials of $H_3PW_{12}O_{40}$ and UiO-66(Zr) have been prepared without the addition of any solvent by one-pot method (Scheme 1). The obtained catalysts were characterized by powder X-ray diffraction (XRD), N_2 adsorption-desorption, scanning electron microscopy (SEM), High resolution high-angle annular dark-field scanning transmission electron microscopy (HR-HAADF), energy dispersive X-ray spectroscopy (EDX), Fourier transform infrared (FT-IR), Time-of-Flight Secondary Ion Mass Spectrometry (ToF-SIMS) and X-ray photoelectron spectroscopy (XPS) techniques. Additionally, their catalytic performance was evaluated in the ODS reactions of benzothiophene (BT),

dibenzothiophene (DBT) and 4,6-dimethyldibenzothiophene (4,6-DMDBT) at room temperature. A possible reaction mechanism was proposed.

2. Experimental

2.1. Materials

$ZrOCl_2 \cdot 8H_2O$, $ZrCl_4$, 1,4-benzenedicarboxylic acid (BDC), phosphotungstic acid ($H_3PW_{12}O_{40}$, PW), N,N'-dimenthylformamide (DMF), hydrogen peroxide (H_2O_2, 30 wt%), 5,5-dimethyl-1-pyrroline N-oxide (DMPO), ethanol, acetonitrile, tertiary butanol, *p*-benzoquinone and *n*-octane were purchased from Sinopharm Chemical Reagent Company. Benzothiophene (BT), dibenzothiophene (DBT) and 4,6-dimethyldibenzothiophene (4,6-DMDBT) were purchased by Aldrich. All chemicals were analytical pure and used without further purification.

2.2. Synthesis of materials

UiO-66(Zr)-green and UiO-66(Zr)-solvent were prepared according to the previous references[31].

Synthesis of PW/UiO-66(Zr)-green: $ZrOCl_2 \cdot 8H_2O$ (1.5 mmol) and BDC (1.5 mmol) were mixed and ground in a mortar by hand for 2 min at room temperature. Then, PW (100, 150, or 200 mg) was added and the resultant mixture was further ground for 8 min. After that, the obtained materials were transferred into 15 mL autoclave and crystallized at 130 °C for 12 h. After cooling to room temperature, the resulting samples were washed with 50 mL ethanol at 70 °C for 6 h once and 10 mL fresh ethanol twice. Finally, the white solids were dried under vacuum for 12 h at 150 °C. The final samples were denoted as PW/UiO-66(Zr)-green-1, PW/UiO-66(Zr)-green, and PW/UiO-66(Zr)-green-2 based on the different weight of added PW in the process of synthesis. Comparatively, a mechanically mixed sample named as PW+UiO-66(Zr)-green was prepared by grinding PW and UiO-66(Zr)-green**.**

Synthesis of PW/UiO-66(Zr)-solvent: 1 mmol $ZrCl_4$ (233 mg) and 1 mmol BDC (166 mg) were dissolved in 30 mL DMF. Then, 300 mg PW was added into the above mixture with stirring. After that, the obtained mixture was transferred into a 40 mL Teflon-lined

autoclave and crystallized at 120 °C for 24 h. After cooling to room temperature, the resultant white solid was washed with 50 mL ethanol at 70 °C for 6 h and 10 mL fresh ethanol twice. Finally, the sample was dried under vacuum for 12 h at 150 °C. The final sample was named as PW/UiO-66(Zr)-solvent.

2.3. Characterization

Powder X-ray diffraction (XRD) patterns were recorded on a Rigaku D/Max-2550 diffractometer equipped with a SolX detector-Cu Ka radiation with wavelength of λ = 1.5418 Å. Nitrogen sorption isotherms were obtained at 77 K on a 3H-2000PS1 Gas Sorption and Porosimetry system. Samples were prepared for measurement after degassing at 423 K under vacuum until a final pressure of 1×10^{-3} Torr was reached. Scanning electron microscopy (SEM) images and energy dispersive X-ray spectroscopy (EDS) elemental mapping were recorded on SUPRA 55 operated with an acceleration voltage of 200 kV. Fourier transform infrared (FT-IR) spectra were recorded on a NicoLET iS10 spectrometer. High resolution high-angle annular dark-field scanning transmission electron microscopy (HR HAADF-STEM) analyses were performed using a FEG TEM/STEM system (Titan Themis FEI) operated at 200 kV, equipped with a monochromator and a probe Cs corrector. For HAADF acquisition, the spot size was 9 with a screen current of ~50 pA and a camera length of 115 mm, corresponding to inner and outer diameters of annular detector of □50 and □200 mrad, respectively. Time-of-Flight Secondary Ion Mass Spectrometry (ToF-SIMS) measurements were performed with a TOF.SIMS 5 spectrometer (ION-TOF GmbH Germany) equipped with a bismuth liquid metal ion gun (LMIG). The compacted samples were bombarded with pulsed Bi^{3+} primary ion beam (25 keV, 0.25 pA) rastered over a 500 × 500 m^2 surface area. With 25 scans and 128x128 pixels, the total primary ion dose does not amount up to 10^{12} ions/cm^2 ensuring static conditions. Charge effects due to primary ion beam were compensated by means of a 20 eV pulsed electron flood gun. Cycle time was fixed at 220µs in order to detect secondary molecular ions up to 4000 m/z. The mass resolution (m/Δm) measured on our spectra was about 6000 at m/z = 232 for WO_3^-. This excellent mass resolution allowed us to identify high m/z ionic fragments by their exact mass and attribution was always confirmed by the simulated isotopic pattern. X-ray photoelectron spectroscopy (XPS) was performed using an ESCALAB 250

spectrometer. AlKα source was used for excitation. Pressure was in the 10^{-10} Torr range during the experiments. The analyser was operated in constant pass energy of 25 eV. Charge compensation was applied to compensate charging effect occurring during the analysis. C1s, O1s, W4f-Zr4p and Zr3d regions were collected. Adventitious carbon was used as internal reference with the C1s peak at binding energy (BE) 284.6 eV. Peak fitting of the experimental photo peaks was carried out using Casa XPS software. Quantification took into account a non-linear Shirley background subtraction.

2.4. Catalytic tests

The ODS reactions were performed by using a three-phase reaction system at room temperature. A calculated amount of BT, DBT or 4,6-DMDBT was dissolved in *n*-octane (with a concentration of 1000, 1000 and 500 ppmw of sulfur for BT, DBT and 4,6-DMDBT, respectively) to act as model fuel. The reaction was performed under air in a closed 40 mL dram vial with a vigorous magnetic stirrer (800 rpm). In a standard run, the activated catalyst (50 mg) was added to model fuel (10 g) and acetonitrile (10 g), and the resulting mixture was stirred for 10 min at room temperature. The catalytic reaction process was initiated by the addition of hydrogen peroxide (H_2O_2, 30 wt. %) as oxidant with an O/S molar ratio of 6:1. The liquids in *n*-octane were withdrawn at regular intervals and analyzed by gas chromatography on an Agilent 7890A GC with an FID detector using a 30 m packed HP5 column. The removal rate (R) of sulfur compounds was calculated according to the equation $R = (1-C_t/C_0) \times 100$ %, where C_0 and C_t stand for the initial concentration and reaction concentration of BT, DBT or 4,6-DMDBT in *n*-octane phase after t minute, respectively.

The reusability of catalyst was carried out at room temperature. After each cycle, the catalyst was recovered by centrifugation, washed with acetonitrile twice, dried under vacuum for 12 h at 150 °C and then reused in a new catalytic cycle under the same reaction conditions.

3. Results and discussion

3.1. Characterization

The XRD results of samples are shown in Fig. 1. As seen, all the PW/UiO-66(Zr)-green samples with different PW contents exhibit well-resolved crystal diffraction peaks, which are in accordance with the crystal structure of UiO-66(Zr). This result indicates that the addition of PW during the synthesis did not prevent the formation of the UiO-66(Zr) structure. Notably, two diffraction peaks appeared at 6.4° and 28.5° of 2 theta degree cannot match well with those of UiO-66(Zr) (Fig. S1). Considering that the peak intensity increased with the addition amount of PW, the two diffraction peaks should result from the PW species although the peak positions shift toward the region of low angle compared with those of PW. This suggests that possibly the PW species exist as aggregated nanoparticles and are encapsulated into the interior of the UiO-66(Zr) crystals and a mutual effect on their crystal structure should occur. Comparatively, PW/UiO-66(Zr)-solvent displays only well-resolved diffraction peaks corresponding to the UiO-66(Zr) structure. This means that the particle size of the PW species in PW/UiO-66(Zr)-solvent seem to be small and their distribution in sample could be relatively homogeneous. Moreover, a mechanically mixed sample (PW+UiO-66(Zr)-green) gives the XRD peaks whose positions are in accordance with those of pure PW besides those of UiO-66(Zr), suggesting that there should be no mutual effect on the crystal structure of this sample.

The N_2 sorption isotherms of all the PW/UiO-66(Zr)-green samples show abrupt increase in the region of low relative pressure (<0.01) and second jump with hysteresis loop at the relative pressure (0.4~0.9), suggesting that they should be hierarchical porous materials (Fig. S2 and S3). In comparison, PW/UiO-66(Zr)-solvent and PW+UiO-66(Zr)-green exhibit type I isotherm and no mesopore size distribution (Fig. 2a and b). The detailed sorption data are listed in Table 1. Obviously, the BET surface areas for the samples prepared by green method gradually decrease with the increase of PW addition amount. However, PW/UiO-66(Zr)-green can still possess high BET surface area (843 m^2/g) when the content of PW in PW/UiO-66(Zr)-green was 14.8 wt%. Actually, the difference in BET surface area is small for PW/UiO-66(Zr)-green, PW/UiO-66(Zr)-solvent and PW+UiO-66(Zr)-green with similar PW content. Differently, PW/UiO-66(Zr)-green (0.57 mL/g) has higher mesopore volume than PW/UiO-66(Zr)-solvent (0.13 mL/g), which should be related to synthetic method. Under the condition of adding no solvent, the concentration of PW should be high and PW species are easy to aggregate into nanoclusters in the synthetic system of the

composite materials. Necessarily, it would occupy some rooms and thus prevent the formation of the perfect crystalline structure of UiO-66(Zr). Because the size of PW nanoclusters (about 1 nm per PW molecule) is big, mesopores can be easily created in the structure of PW/UiO-66(Zr)-green.

FT-IR spectra of various samples are shown in Fig. 3 and S4. All the samples with the addition of PW exhibit an absorption band at 1081 cm^{-1} assigned to the asymmetric vibration of the P=O bond from PW and three absorption bands at 982, 891, and 802 cm^{-1} corresponding to the asymmetric vibrations of the terminal W=O, corner and edge share of W-O-W bonds, respectively[32-34]. Comparatively, those absorption bands are absent in the samples of UiO-66(Zr)-solvent and UiO-66(Zr)-green. These results suggest that PW should exist in the composite materials of PW and UiO-66(Zr).

The SEM results are shown in Fig. 4 and S5. Clearly, UiO-66(Zr)-green exhibits a flake-like morphology and is mainly composed of crystals with a size of 50×150 nm (Fig. 4a). With the addition of PW, the crystal tends to aggregate each other and the average particle size is larger than that of UiO-66(Zr)-green (Fig. 4b and S5). Comparatively, UiO-66(Zr)-solvent shows a morphology of spherical shape and its average particle size is about 200 × 200 nm (Fig. 4c). Similarly, after the introduction of PW, the crystal size of PW/UiO-66(Zr)-solvent is larger than that of UiO-66(Zr)-solvent (Fig. 4d). Moreover, Fig. 4e and 4f showed the EDS patterns of PW/UiO-66(Zr)-green and PW/UiO-66(Zr)-solvent. The results proved the presence of W species in both samples.

To clearly know the location and distribution of PW in samples, TEM images are taken (Fig. 5). As seen in Fig. 5a, the distribution of the element W in PW/UiO-66(Zr)-green is not homogeneous and even no element W is detected in some crystal particles. The results from EDS element mapping can further demonstrate this point (Fig. 5b and S6). Comparatively, the element W in PW/UiO-66(Zr)-solvent is uniformly distributed (Fig. 5c, d and Fig. S7). Moreover, the particle size of PW in PW/UiO-66(Zr)-green is bigger than that in PW/UiO-66(Zr)-solvent. These results reveal that PW species in PW/UiO-66(Zr)-green tend to form nanoclusters.

The XPS results of various samples are shown in Fig. 6. As seen, PW/UiO-66(Zr)-green and PW/UiO-66-solvent present the binding energies of element W, suggesting that PW should exist in the UiO-66(Zr) materials. The binding energies of Zr $3d_{5/2}$, O

1s, and C 1s for all the samples are almost the same (Fig. S8-10). However, the binding energy of W 4f is somewhat different (Fig. 6a). As for pure PW, two binding energies at 36.1 and 38.2 eV is ascribed to W $4f_{7/2}$ and W $4f_{5/2}$, respectively. As for the composite materials of PW and UiO-66(Zr), the two binding energies shift toward low values (Fig. 6b). This means that the electron density of W in these composites was possibly increased after PW species captured electrons, suggesting that the electron transfer between UiO-66(Zr) and PW species might occur[35-37].

The quantitative analysis from XPS results (Table S1) shows that the surface chemical composition of UiO-66(Zr) are in accordance with the chemical structure ($Zr_6O_4(OH)_4(bdc)_6$) and the structure is maintained for PW/UiO-66(Zr)-green and PW+UiO-66-green catalysts. It also should be related to the loss of organic linker in PW/UiO-66(Zr)-green and PW+UiO-66(Zr)-green as demonstrated for pure UiO-66(Zr)-green MOF in our previous works[31]. An excess of carbon, which could be attributed to lower loss of organic linker, is observed for PW/UiO-66(Zr)-solvent. The nW/nZr atomic ratio shows that the surface PW content is close to the bulk content for PW/UiO-66-green, compatible with an insertion of PW in the UiO-66(Zr) MOF framework or very small PW crystallites. A depletion of PW is observed at the surface for the mechanical mixture PW+UiO-66-green and PW/UiO-66(Zr)-solvent. It is in accordance with the large PW crystallites in contact with the UiO-66(Zr) solids.

PW/UiO-66(Zr)-green and PW/UiO-66(Zr)-solvent were analyzed by ToF-SIMS, in order to compare the interaction between HPW and support depending on the preparation method. Indeed, ToF-SIMS probes the top layers (1-3 nm) of the catalysts and allows obtaining molecular information about surface and interfaces. Fragments recorded are listed in Supplementary Information. For both catalysts, fragments containing W and Zr were recorded, $WZrO^{4+}$ and WZr_2O^{6+}, as illustrated in Fig. S11, the simulation of its isotope pattern confirming their identification. Considering that they contain both Zr and W, their presence indicated a close interaction between HPW and the UiO-66(Zr). However, it appears clearly that these mixed fragments are much more numerous in the PW/UiO-66(Zr)-green sample, proving that the without solvent method promotes the interaction between HPW and the support. It can be beneficial for the lifetime of the catalyst, thus avoiding leaching during reaction

3.2. Catalytic evaluation

The catalytic performance of the PW/UiO-66(Zr)-green samples with different PW contents were firstly evaluated by ODS of DBT at room temperature. As shown in Fig. S12, the removal of DBT over PW/UiO-66(Zr)-green-1, PW/UiO-66(Zr)-green and PW/UiO-66(Zr)-green-2 reached 91.5 %, 99.7 % and 98.2 % after a reaction time of 25 min, respectively. Notably, PW/UiO-66(Zr)-green displays best ODS performance among the three samples, which might result from a suitable combination of PW content and mesoporosity in PW/UiO-66(Zr)-green. Surprisingly, it is inactive when pure PW is used as ODS catalyst at room temperature (The removal of about 55% DBT resulted from the extraction by acetonitrile). Similarly, PW/UiO-66(Zr)-solvent also displays poor reactivity at the same reaction conditions. Interestingly, PW+UiO-66(Zr)-green exhibited better ODS performance than PW/UiO-66(Zr)-solvent, suggesting that probably the synergistic effect of PW and defective UiO-66(Zr)-green occurred (Fig. 7). Furthermore, in order to clarify whether DBT was oxidized or absorbed on PW/UiO-66(Zr)-green, the components in oil phase and acetonitrile phase after reaction were analyzed by GC-MS. These results show that only dibenzothiophene sulfone ($DBTO_2$) can be detected in acetonitrile phase, verifying that DBT has been really oxidized into $DBTO_2$ over PW/UiO-66(Zr)-green (Fig. S13).

To make a comprehensive comparison, the catalytic activities of several representative POM/MOF composites as catalysts for DBT removal are given in Fig. 8 and some data are listed Table S2. Obviously, the TOF number over reported catalysts is below 50 h^{-1} even if high reaction temperature is used. However, the TOF number over PW/UiO-66(Zr)-green can reach 221 h^{-1} although the reaction runs at room temperature. To our best knowledge, this value is the highest among the reported ODS catalysts under the reaction condition of room temperature. Considering that PW/UiO-66(Zr)-green could be an excellent ODS catalyst, the effect of some factors on its catalytic performance was investigated as follows.

3.3. Effect of reaction temperature

The effect of reaction temperature on the catalytic performance of PW/UiO-66(Zr)-green is shown in Fig. 9a. Obviously, the ODS activity increases with reaction

temperature. When the reaction temperature is increased to 50 °C, the removal of DBT reaches 99.8% after a reaction time of 10 min. The reaction rate constants at different temperatures are calculated according to the pseudo-first-order kinetics: $\ln (C_0/C_t) = kt$ and $\ln k = -E_a/RT$, where C_0 and C_t represent the DBT concentration at the initial and t time, while k and E_a represent the rate constant and the activation energy, respectively. The linear plots of $\ln(C_0/C_t)$ versus reaction time are shown in Fig. S14 and the data are listed in Table S3. After calculation by Arrhenius equation, the apparent activation energy over PW/UiO-66(Zr)-green is 30.5 kJ/mol (Fig. 9b). The value is low compared with the data from the literatures[38-40].

3.4. Effect of O/S molar ratio and DBT concentration

The effect of O/S molar ratio on the catalytic performance of PW/UiO-66(Zr)-green is shown in Fig. 10a. Obviously, the ODS activity of PW/UiO-66(Zr)-green decreases with the O/S molar ratio. When the O/S molar ratio is 2:1, the removal of DBT can reach 80% after a reaction time of 30 min. Meanwhile, the oxidant efficiency increases with O/S molar ratio to 88.1%. Additionally, the effect of DBT concentration is also investigated. As shown in Fig. 10b, the removal of DBT is completed within 20 min when the concentration of DBT is 500 ppm. When the concentration of DBT is increased to 1500 ppm, relatively long reaction time is needed for the complete removal of DBT. However, PW/UiO-66(Zr)-green is still active. The removal of DBT may reach 99.7% after a reaction time of 40 min at room temperature.

3.5. Effect of sulfur substrate

The effect of sulfur substrate on the catalytic performance of PW/UiO-66(Zr)-green is studied by the ODS reactions of BT, DBT, and 4,6-DMDBT. As seen in Fig. 11, the removal of 4,6-DMDBT over PW/UiO-66(Zr)-green is 99.8 % after a reaction time of 25 min, suggesting that PW/UiO-66(Zr)-green has great potential in deep ODS of fuel oil. BT was the most difficult to oxidize, with 81 % conversion at 25 min, in agreement with the lower electron density on the sulfur atom (5.739) compared to DBT and 4,6-DMDBT (5.758 and 5.760 respectively)[29, 39].

3.6. Reusability and structural stability of catalyst

The reusability of PW/UiO-66(Zr)-green is also evaluated by the ODS reaction of DBT. After each cycle, the catalyst is recovered by centrifugation, washing with acetonitrile, and reused in the next cycle under the same reaction conditions. As shown in Fig. 12, PW/UiO-66(Zr)-green could still maintain high catalytic ODS activity after four cycles. The results indicate that PW/UiO-66(Zr)-green is a heterogeneous catalyst and can be reused. Additionally, the structural stability of PW/UiO-66(Zr)-green after reuse is also assessed by XRD and N_2 absorption techniques. As seen in Fig. S15, the XRD patterns of the reused sample are in accordance with those of the fresh one. Moreover, the reused PW/UiO-66(Zr)-green displays similar N_2 sorption isotherms (BET surface area of 833 m^2/g) to the fresh one (843 m^2/g) (Fig. S16), proving that the structure of PW/UiO-66(Zr)-green is stable after reuse.

3.7. Proposed reaction mechanism

To explore the reaction mechanism, quenching experiments were conducted. Generally, $HO^{\bullet}$ or $O_2^{\bullet-}$ is considered to be catalytic active species in the reaction. It is known that tertiary butanol or *p*-benzoquinone is a good quencher of $HO^{\bullet}$ or $O_2^{\bullet-}$, respectively[41-43]. As shown in Fig. 13, when PW/UiO-66(Zr)-green is removed from the reaction system after a reaction time of 10 min, the removal of DBT remained constant after a reaction time of 25 min. With the addition of tertiary butanol, the removal content of DBT is slightly reduced, indicating that $HO^{\bullet}$ should exist in the catalytic system. Moreover, the addition of *p*-benzoquinone decreases the removal of DBT from 99.8 % to 96.3 % after the same reaction time, suggesting that $O_2^{\bullet-}$ should also play a positive role in catalytic performance. Furthermore, electron paramagnetic resonance (EPR) spin-trap method was utilized to probe the formation of radicals with 5,5-dimethyl-1-pyrroline N-oxide (DMPO) as traps. As seen in Fig. 14, the strong characteristic four peaks of DMPO-$O_2^{\bullet-}$ signals with relative intensities of about 1:1:1:1 were observed in the mixture of PW/UiO-66(Zr)-green (5 mg), H_2O_2 (0.5 mL), and DMPO (50 μL), confirming the formation of $O_2^{\bullet-}$ radicals. However, it is difficult to know if the $HO^{\bullet}$ radicals were generated because of EPR signals of DMPO-$O_2^{\bullet-}$ and

DMPO-HO$^{\bullet}$ overlap. Interestingly, the addition of both tertiary butanol and *p*-benzoquinone can greatly inhibit the further removal of DBT, demonstrating that both HO$^{\bullet}$ and $O_2^{\bullet-}$ radicals should be generated in the ODS reaction system.

Based on the above experimental results, a possible reaction mechanism was proposed over PW/UiO-66(Zr)-green (Scheme 2). The DBT molecule in model oil was extracted into acetonitrile phase with the catalyst and H_2O_2. Then, DBT and H_2O_2 can be adsorbed in the pores of PW/UiO-66(Zr)-green. It would be helpful for promoting the interaction between substrate, catalyst and oxidants. Meanwhile, partially adsorbed H_2O_2 decomposed into HO$^{\bullet}$ radicals through electron transfer by the Zr-OH_2 sites in UiO-66(Zr)[29, 44]. Part of H_2O_2 could interact with the W sites in PW species into W(VI)-peroxo and then form $O_2^{\bullet-}$ radicals. Both radicals can oxidize DBT into $DBTO_2$ [14, 45-47]. Therefore, the existence of two types of active centers from PW species and defective UiO-66(Zr) plays a vital role in the formation of radicals, which should be responsible for the highly efficient ODS performance at room temperature.

In addition, the accessibility of active sites is also important. As shown in Figure 7, PW/UiO-66(Zr)-solvent is not active at room temperature in the ODS reaction of DBT although PW species are homogeneously distributed in the sample, which should be related to the accessibility of active sites. As seen from N_2 sorption results, PW/UiO-66(Zr)-solvent had much lower pore volume than PW/UiO-66(Zr)-green and did not exhibit mesopore distribution. This means that it is difficult for sulfur compounds to access the active PW species in PW/UiO-66(Zr)-solvent due to the limitation of micropore size and the lack of mesoporosity. This could be main reason why PW/UiO-66(Zr)-solvent showed poorer ODS reactivity than PW/UiO-66(Zr)-green.

4. Conclusions

In summary, the composite materials of PW and UiO-66(Zr) have successfully been prepared without the addition of any solvent. The results from XRD and TEM indicate that PW species in PW/UiO-66(Zr)-green mainly consisted of nanoclusters. Nitrogen sorption measurement revealed that the obtained composite materials possessed hierarchical porosity with high mesopore volume. As ODS catalysts, they exhibited extraordinary catalytic performance in the ODS reactions of DBT and 4,6-DMDBT at

room temperature. The TOF number for the removal of DBT reached 221.4 h^{-1}, which is much higher than that of the reported catalysts. Such outstanding catalytic performance could be mainly attributed to easy accessibility of active sites and the existence of two types of active centers from PW species and defective UiO-66(Zr). Due to the simplification and environmental friendliness of synthetic processes, it will be of significance for potential applications.

Acknowledgments: The authors acknowledge the financial support from Key Laboratory of Functional Inorganic Material Chemistry (Heilongjiang University), Ministry of Education, and Open Funding from the State Key Lab of Inorganic Synthesis and Preparative Chemistry, Jilin University. Chevreul institute (FR 2638), Ministère de l'Enseignement Supérieur et de la Recherche and Région Hauts-de-France are acknowledged for supporting this work.

References

[1] A. Stanislaus, A. Marafi, M. S. Rana, Catal. Today 2010, 153, 1-68.

[2] Y. Y. Sun, R. Prins, Angew. Chem. Int. Ed., 2008, 47, 8478-8481.

[3] X. Y. Zeng, X. Y. Xiao, J. Y. Chen, H. L. Wang, Appl. Catal. B Environ., 2019, 248, 573-586.

[4] Z. Li, D. Liu, Z. Men, L. Song, Y. Lv, P. Wu, B. Lou, Y. Zhang, N. Shi, Q. Chen, Green. Chem., 2018, 20, 3112-3120.

[5] J. Xiao, S. Sitamraju, Y. Chen, S. Watanabe, M. Fujii, M. Janik, C. Song, AICHE J. 2015, 61, 631-639.

[6] A. A. Toutov, M. Salata, A. Fedorov, Y. F. Yang, Y. Liang, R. Cariou, K. N. Betz, E. P. A. Couzijn, J. W. Shabaker, K. N. Houk, R. H. Grubbs, Nat. Energy 2017, 2, 17008.

[7] Z. Vit, D. Gulkova, L. Kaluza, J. Kupcik, Appl. Catal. B Environ., 2015, 179, 44-53.

[8] E. M. Morales-Valencia, C. O. Castillo-Araiza, S. A. Giraldo, V. G. Baldovino-Medrano, ACS Catal., 2018, 8, 3926-3942.

[9] X. L. Wang, J. L. Mei, Z. Zhao, P. Zheng, Z. T. Chen, D.W. Gao, J. Y. Fu, J. Y. Fan, A. J. Duan, C. M. Xu, ACS Catal., 2018, 8, 1891-1902.

[10] L. van Haandel, G. M. Bremmer, E. J. M. Hensen, T. Weber, J. Catal., 2017, 351, 95-106.

[11] S. W. Li, Z. Yang, R. M. Gao, G. Zhang, J. S. Zhao, Appl. Catal. B: Environ., 2018, 221, 574-583.

[12] K. Y. Leng, X. L. Li, G. Ye, Y. C. Du, Y. Y. Sun, W. Xu, Catal. Sci. Technol., 2016, 6, 7615-7622.

[13] G. Ye, H. Qi, X. L. Li, K. Y. Leng, Y. Y. Sun, W. Xu, ChemPhysChem, 2017, 18, 1903-1908.

[14] C. M. Granadeiro, S. O. Ribeiro, M. Karmaoui, R. Valenca, J. C. Ribeiro, B. Castro de, L. Cunha-Silva, S. S. Balula, Chem. Commun., 2015, 51, 13818-13821.

[15] C. X. Shi, W. X. Wang, N. Liu, X. Y. Xu, D. H. Wang, M. H. Zhang, P. C. Sun, T. H. Chen, Chem. Commun., 2015, 51, 11500-11503.

[16] H. Y. Liu, S. X. Bao, Z. T. Cai, T. F. Xu, N. Li, L. L. Wang, H. X. Chen, W. Y. Lu, W. X. Chen, Chem. Eng. J., 2017, 317, 1092-1098.

[17]L. W. Hao, L. L. Sun, T. Su, D. M. Hao, W. P. Liao, C. L. Deng, W. Z. Ren, Y. M. Zhang, H. Y. Lü, Chem. Eng. J., 2019, 358, 419-426.

[18] C. T. Buru, A. E. Platero-Prats, D. G. Chica, M. G. Kanatzidis, K. W. Chapman, O. K. Farha, J. Mater. Chem. A, 2018, 6, 7389-7394.

[19] I. V. Kozhevnikov, Chem. Rev., 1998, 98, 171-198.

[20] J. Ye, C. Wu, Dalton Trans., 2016, 45, 10101-10112.

[21] S. M. Lauinger, J. M. Sumliner, Q. Yin, Z. Xu, G. Liang, E. N. Glass, T. Lian, C. L. Hill, Chem. Mater., 2015, 27, 5886-5891.

[22] C. L. Hill, Compr. Coord. Chem. II, 2004, 4, 679-759.

[23] P. Gouzerh, A. Proust, Chem. Rev., 1998, 98, 77-112.

[24] D. L. Long, E. Burkholder, L. Cronin, Chem. Soc. Rev., 2007, 36, 105-121.

[25] M. Genovese, K. Lian, J. Mater. Chem. A, 2017, 5, 3939-3947.

[26] M. Gomez-mingot, C. Roch-marchal, B. Lassalle-kaiser, P. Mialane, M. Fontecave, C. Mellot-draznieks, A. Dolbecq, J. Am. Chem. Soc., 2018, 140, 3613-3618

[27] W. Salomon, C. Roch-Marchal, P. Mialane, P. Rouschmeyer, C. Serre, M. Haouas, F. Taulelle, S. Yang, L. Ruhlmann, A. Dolbecq, Chem. Commun., 2015, 51, 2972-2975.

[28] X. S. Wang, L. Li, J. Liang, Y. B. Huang, R. Cao, ChemCatChem., 2017, 9, 971-979.

[29] Z. J. Lin, H. Q. Zheng, J. Chen, W. E Zhuang, Y. X. Lin, J. W. Su, Y. B. Huang, R. Cao, Inorg. Chem., 2018, 57, 13009-13019.

[30] Y. L. Peng, J. Y. Liu, H. F. Zhang, D. Luo, D. Li, Inorg. Chem. Front., 2018, 5, 1563-1569.

[31] G. Ye, D. Zhang, X. F. Li, K. Y. Leng, W. J. Zhang, J. Ma, Y. Y. Sun, W. Xu and S. Q. Ma, ACS Appl. Mater. Interfaces, 2017, 9, 34937-34943.

[32] S. Y. Jia, Y. F. Zhang, Y. Liu, F. X. Qin, H. T. Ren, S. H. Wu, J. Hazard. Mater., 2013, 262, 589–597.

[33] A. Afzalinia, A. Mirzaie, A. Nikseresht, T. Musabeygi, Ultrason. Sonochem., 2017, 34, 713-720.

[34] K. X. Li, L. S. Yan, Z. X. Zeng, S. L. Luo, X. B. Luo, X.M. Liu, H. Q. Guo, Y. H. Guo, Appl. Catal. B: Environ., 2014, 156-157, 141-152.

[35] W. J. Zhou, T. L. Xiong, C. H. Shi, J. Zhou, K. Zhou, N. W. Zhu, L. G. Li, Z. H. Tang, S. W. Chen, Angew. Chem. Int. Ed., 2016, 55, 8416.

[36] X. You, L. L. Yu, F. F. Xiao, S. C. Wu, C. Yang, J. H. Cheng, Chem. Eng. J., 2018, 335, 812-821.

[37] P. C. Meng, H. M. Heng, Y. H. Sun, J. H. Huang, J. P. Yang, X. Liu, Appl. Catal. B: Environ., 2018, 226, 487–498.

[38] L. W. Zhang, S. H. Wu, Y. Liu, F. F. Wang, X. Han, H. Y. Shang, Appl. Organometal. Chem. 2016, 30, 684-690.

[39] A. Bazyari, A. A. Khodadadi, A. H. Mamaghani, J. Beheshtian, L. T. Thompson, Y. Mortazavi, Appl. Catal. B: Environ., 2016, 180, 65-77.

[40] C. Shen, Y. J. Wang, J. H. Xu, G. S. Luo, Green Chem., 2016, 18, 771-781.

[41] A. Dhakshinamoorthy, S. Navalon, M. Alvaro and H. Garcia, ChemSusChem, 2012, 5, 46-64.

[42] A. Santiago-Portillo, S. Navalon, F. G. Cirujano, F. X. Llabres i Xamena, M. Alvaro, H. Garcia, ACS Catal., 2015, 5, 3216-3224.

[43] R. Martin, S. Navalon, J. J. Delgado, J. J. Calvino, M. Alvaro, H. Garcia, Chem. Eur. J., 2011, 17, 9494-9502.

[44] H. Q. Zheng, C. Y. Liu, X. Y. Zeng, J. Chen, J. Lü, R. G. Lin, R. Cao, Z. J. Lin, J. W. Su, Inorg. Chem., 2018, 57, 9096-9104.

[45] S. Ribeiro, C. M. Granadeiro, P. Silva, F. A. Almeida Paz, F. F. de Biani, L. Cunha-Silva, S. S. Balula, Catal. Sci. Technol., 2013, 3, 2404-2414.

[46] B. Bertleff, J. Claußnitzer, W. Korth, P. Wasserscheid, A. Jess, J. Albert, ACS Sustainable Chem. Eng., 2017, 5, 4110-4118.

[47] A. Gómez-Paricio, A. Santiago-Portillo, S. Navalón, P. Concepción, M. Alvaroa, H. Garcia, Green Chem., 2016, 18, 508-515.

Captions to Figures

Scheme 1. Diagram about the synthetic processes of PW/UiO-66(Zr)-green.

Scheme 2. Proposed reaction mechanism of PW/UiO-66(Zr)-green in ODS reactions at room temperature.

Figure 1. XRD patterns of various samples.

Figure 2. (a) N_2 sorption isotherms and (b) pore size distribution curves of various samples.

Figure 3. FT-IR spectra of (a) UiO-66(Zr)-green, (b) PW/UiO-66(Zr)-green, (c) UiO-66(Zr)-solvent, (d) PW/UiO-66(Zr)-solvent, (e) PW.

Figure 4. SEM images of (a) UiO-66(Zr)-green, (d) PW/UiO-66(Zr)-green, (c) UiO-66(Zr)-solvent, (d) PW/UiO-66(Zr)-solvent, and EDS patterns of PW/UiO-66(Zr)-green (e) and PW/UiO-66(Zr)-solvent (f).

Figure 5. TEM images of (a) and (b) PW/UiO-66(Zr)-green, (d) and (e) PW/UiO-66(Zr)-solvent, and the corresponding EDS mapping of PW/UiO-66(Zr)-green (c) and PW/UiO-66(Zr)-solvent (f).

Figure 6. XPS spectra of various samples: (a) survey spectrum and (b) W 4f.

Figure 7. Catalytic activities of different catalysts with reaction time in ODS of DBT at room temperature.

Figure 8. The TOF number over various catalysts in the ODS reaction of DBT.

Figure 9. Effect of reaction temperature on catalytic performance of PW/UiO-66(Zr)-green and arrhenius plot.

Figure 10. Effect of different O/S molar ratio (a), and DBT content (b) on catalytic performance of PW/UiO-66(Zr)-green.

Figure 11. Effect of sulfur substrate on catalytic performance of PW/UiO-66(Zr)-green.

Figure 12. Reusability of PW/UiO-66(Zr)-green in the ODS reaction of DBT.

Figure 13. Leaching test and quenching experiments in the ODS reaction of DBT over PW/UiO-66(Zr)-green.

Figure 14. EPR spectrum of 5 mg PW/UiO-66(Zr)-green, 500 μL CHP and 50 μL DMPO.

Table 1. Textural properties of various samples.

Samples	W content (wt.%)[a]	BET surface area (m^2/g)	Micropore volume (mL/g)[b]	Mesopore volume (mL/g)[c]
UiO-66(Zr)-green	--	1131	0.48	0.46
PW/UiO-66(Zr)-green-1	11.9	991	0.44	1.01
PW/UiO-66(Zr)-green	14.8	843	0.35	0.57
PW/UiO-66(Zr)-green-2	17.9	693	0.30	0.62
UiO-66(Zr)-solvent	--	989	0.43	0.19
PW/UiO-66(Zr)-solvent	14.4	746	0.32	0.13
PW+UiO-66(Zr)-green	15.0	873	0.39	0.40

[a] Measured by EDS; [b] HK method; [c] BJH method.

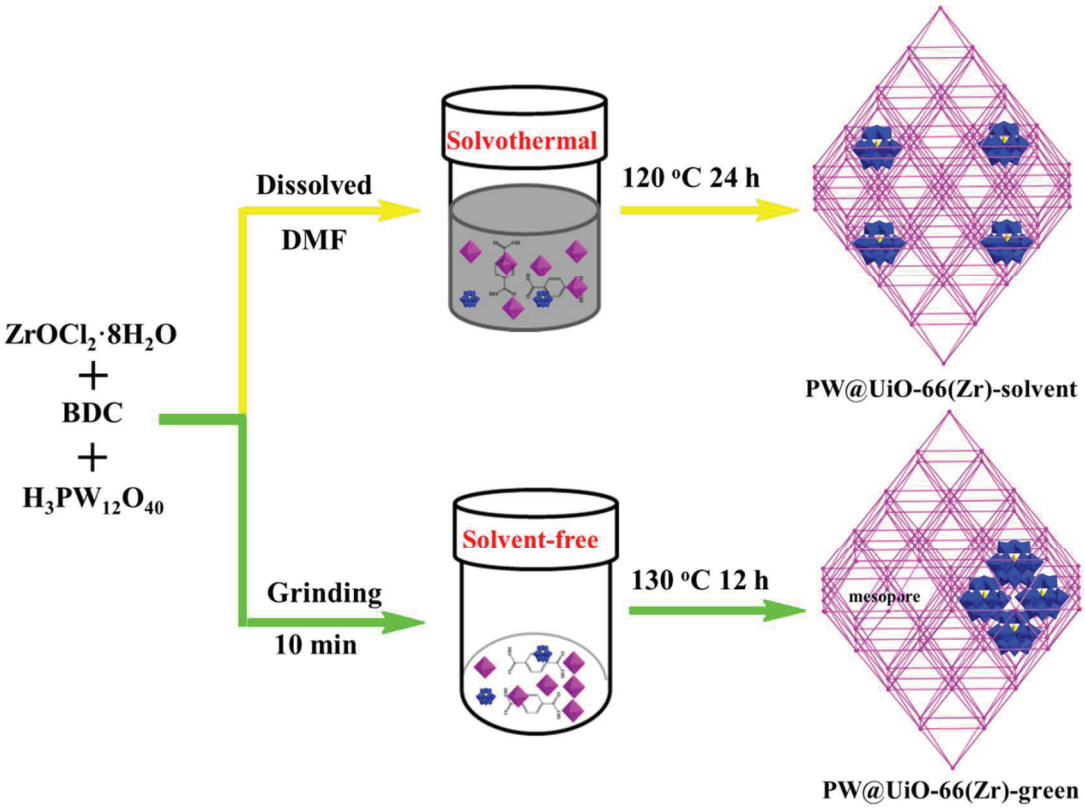

Scheme 1

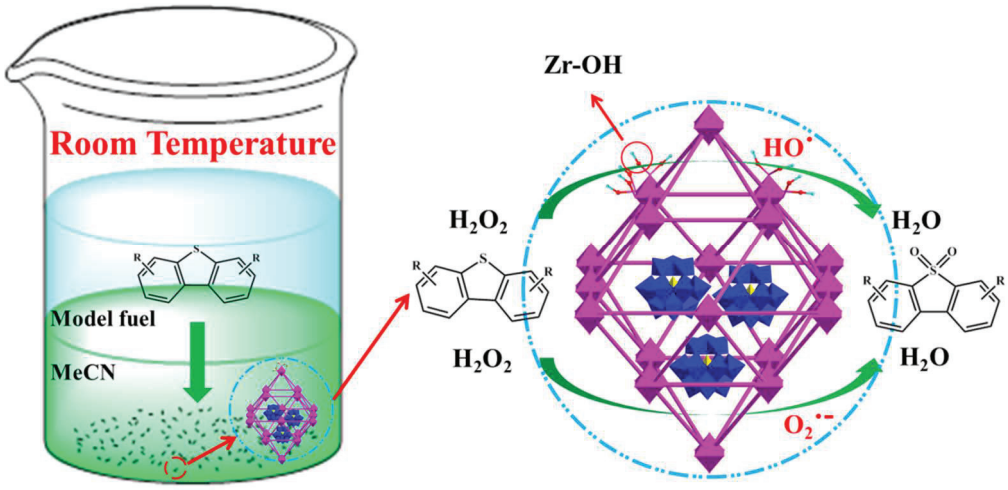

Scheme 2

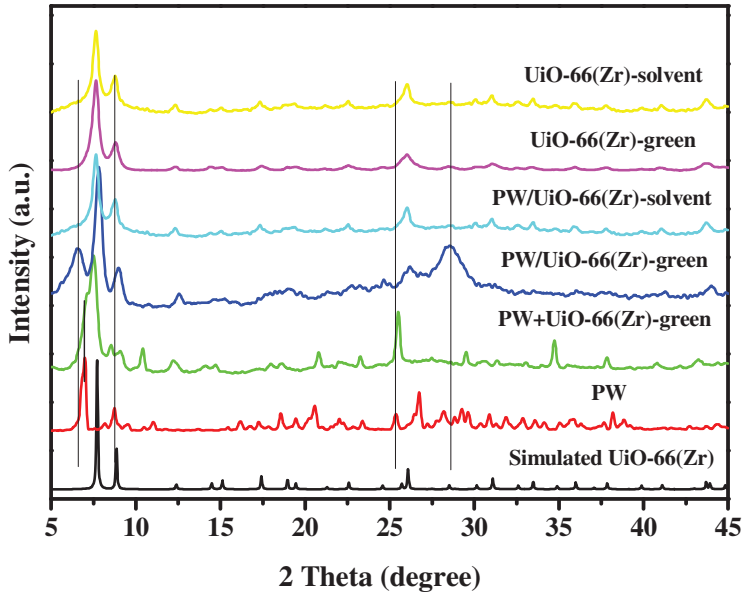
UiO-66(Zr)-solvent
UiO-66(Zr)-green
PW/UiO-66(Zr)-solvent
PW/UiO-66(Zr)-green
PW+UiO-66(Zr)-green
PW
Simulated UiO-66(Zr)
Intensity (a.u.)
5
10
15
20
25
30
35
40
45
2 Theta (degree)

Figure 1

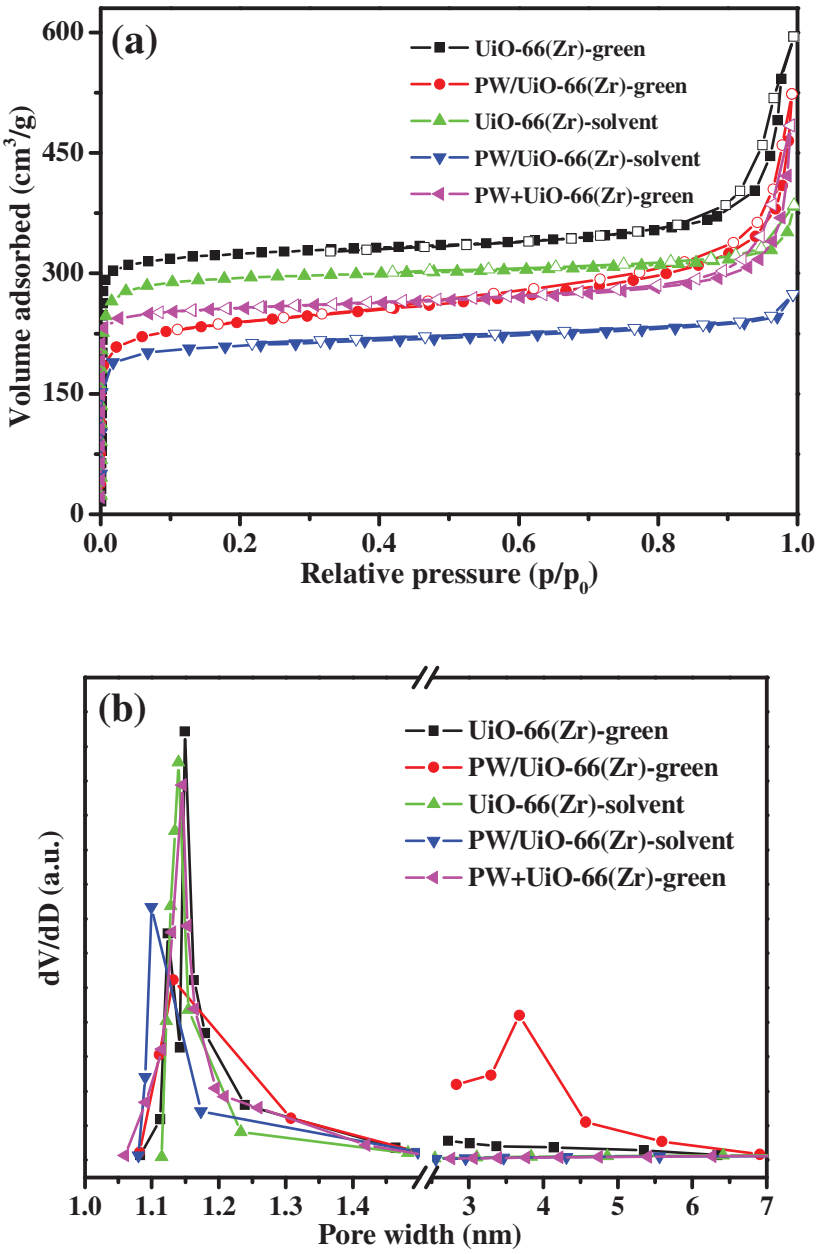
(a)
UiO-66(Zr)-green
PW/UiO-66(Zr)-green
UiO-66(Zr)-solvent
PW/UiO-66(Zr)-solvent
PW+UiO-66(Zr)-green
Volume adsorbed (cm3/g)
Relative pressure (p/p0)
0
150
300
450
600
0.0
0.2
0.4
0.6
0.8
1.0
(b)
dV/dD (a.u.)
Pore width (nm)
1.0
1.1
1.2
1.3
1.4
3
4
5
6
7

Figure 2

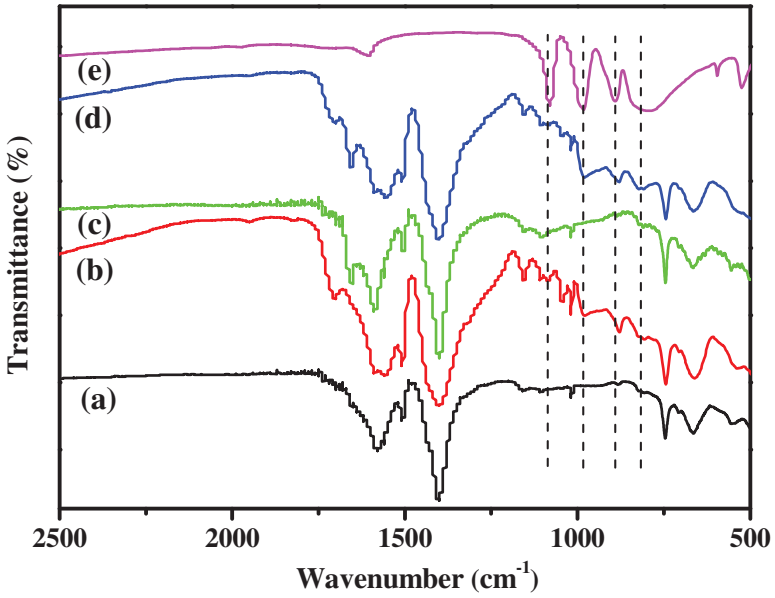
(e)
(d)
(c)
(b)
(a)
Transmittance (%)
2500
2000
1500
1000
500
Wavenumber (cm-1)

Figure 3

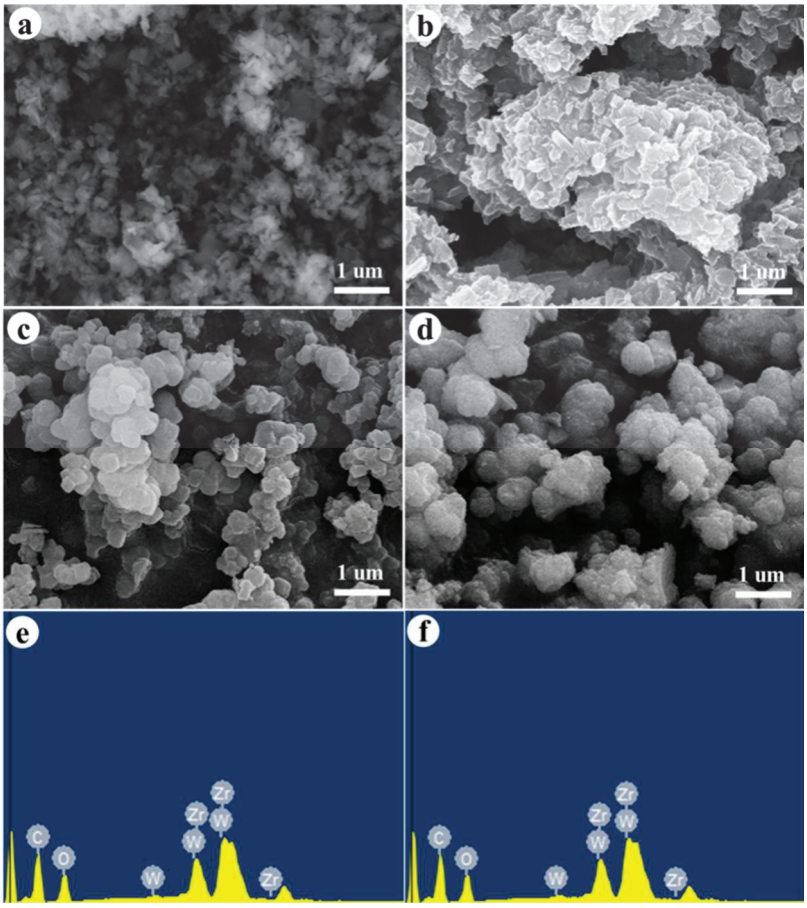

Figure 4

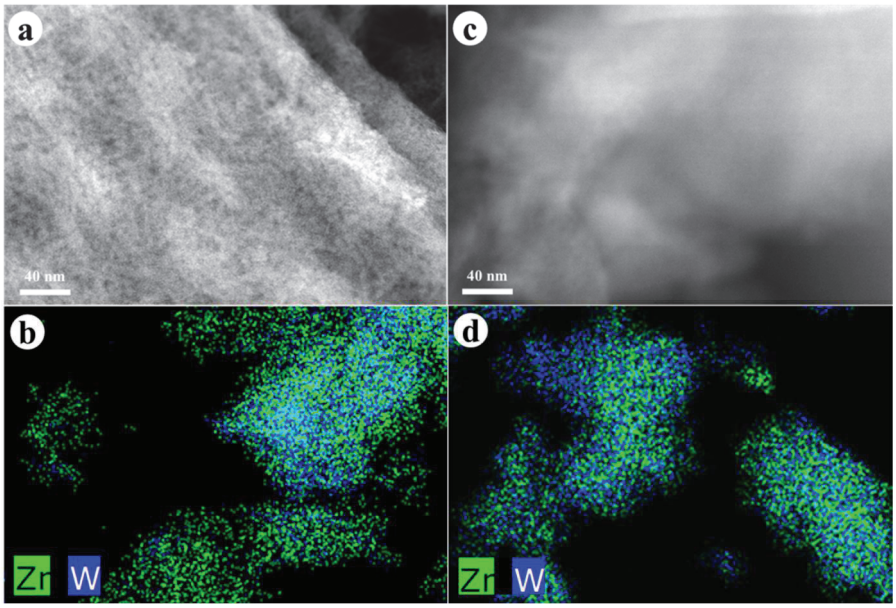

Figure 5

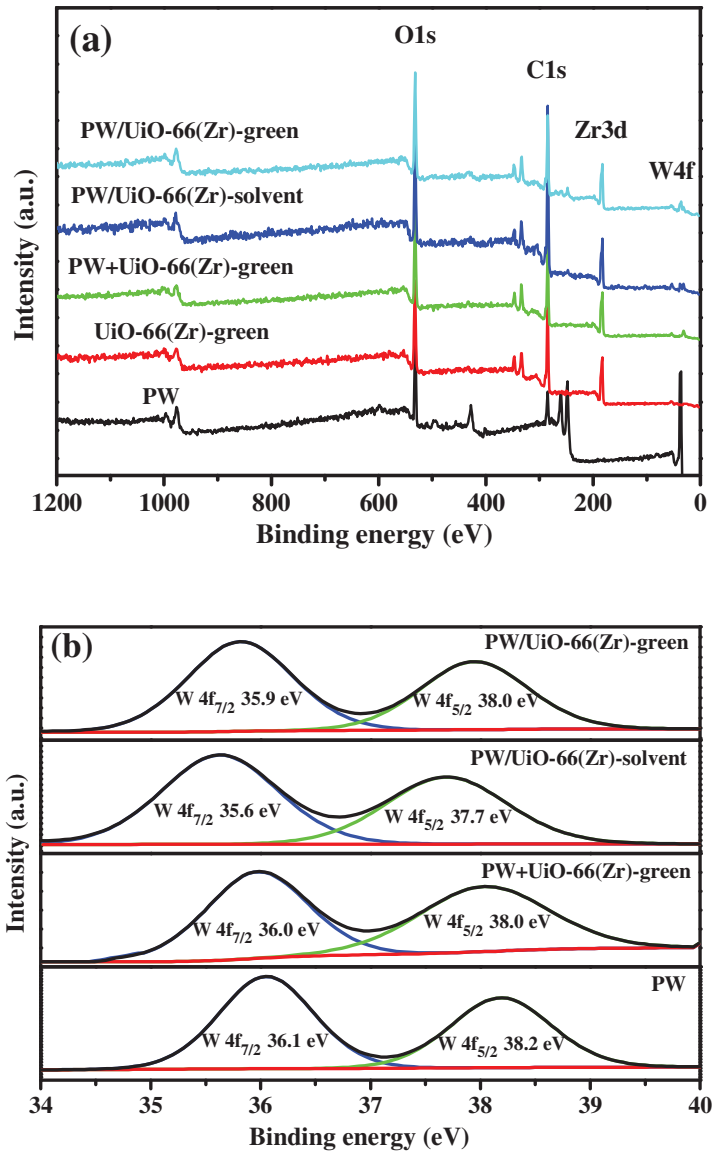
(a)
O1s
C1s
Zr3d
W4f
PW/UiO-66(Zr)-green
PW/UiO-66(Zr)-solvent
PW+UiO-66(Zr)-green
UiO-66(Zr)-green
PW
Intensity (a.u.)
1200
1000
800
600
400
200
0
Binding energy (eV)
(b)
PW/UiO-66(Zr)-green
W 4f7/2 35.9 eV
W 4f5/2 38.0 eV
PW/UiO-66(Zr)-solvent
W 4f7/2 35.6 eV
W 4f5/2 37.7 eV
PW+UiO-66(Zr)-green
W 4f7/2 36.0 eV
W 4f5/2 38.0 eV
PW
W 4f7/2 36.1 eV
W 4f5/2 38.2 eV
Intensity (a.u.)
34
35
36
37
38
39
40
Binding energy (eV)

Figure 6

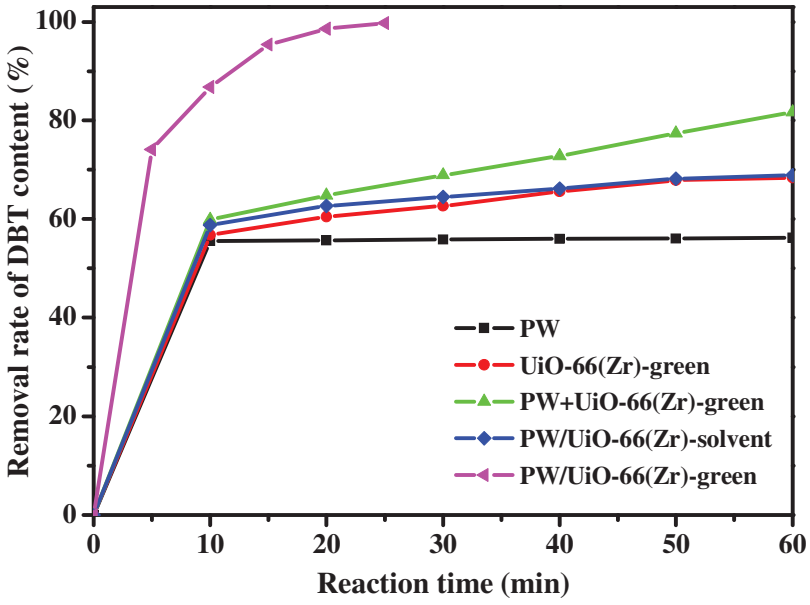
Removal rate of DBT content (%)
Reaction time (min)
0
20
40
60
80
100
0
10
20
30
40
50
60
PW
UiO-66(Zr)-green
PW+UiO-66(Zr)-green
PW/UiO-66(Zr)-solvent
PW/UiO-66(Zr)-green

Figure 7

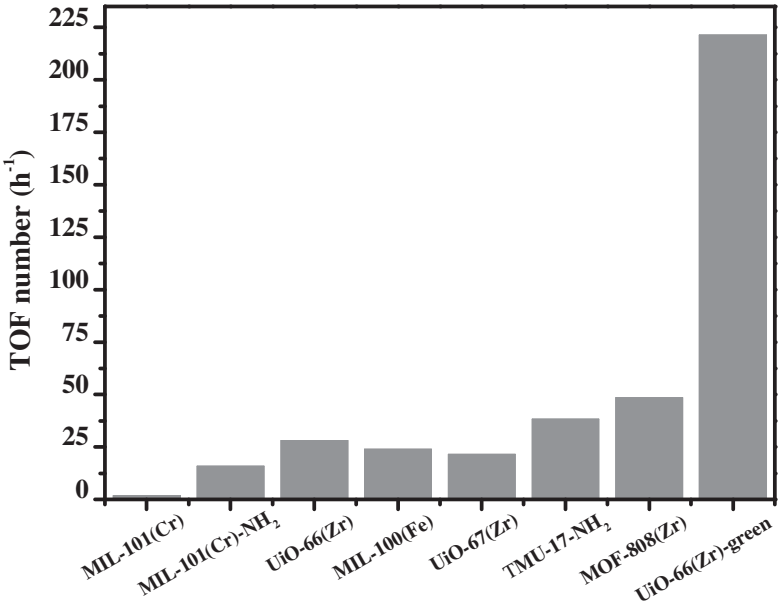
TOF number (h^{-1})
225
200
175
150
125
100
75
50
25
0
MIL-101(Cr)
MIL-101(Cr)-NH_2
UiO-66(Zr)
MIL-100(Fe)
UiO-67(Zr)
TMU-17-NH_2
MOF-808(Zr)
UiO-66(Zr)-green

Figure 8

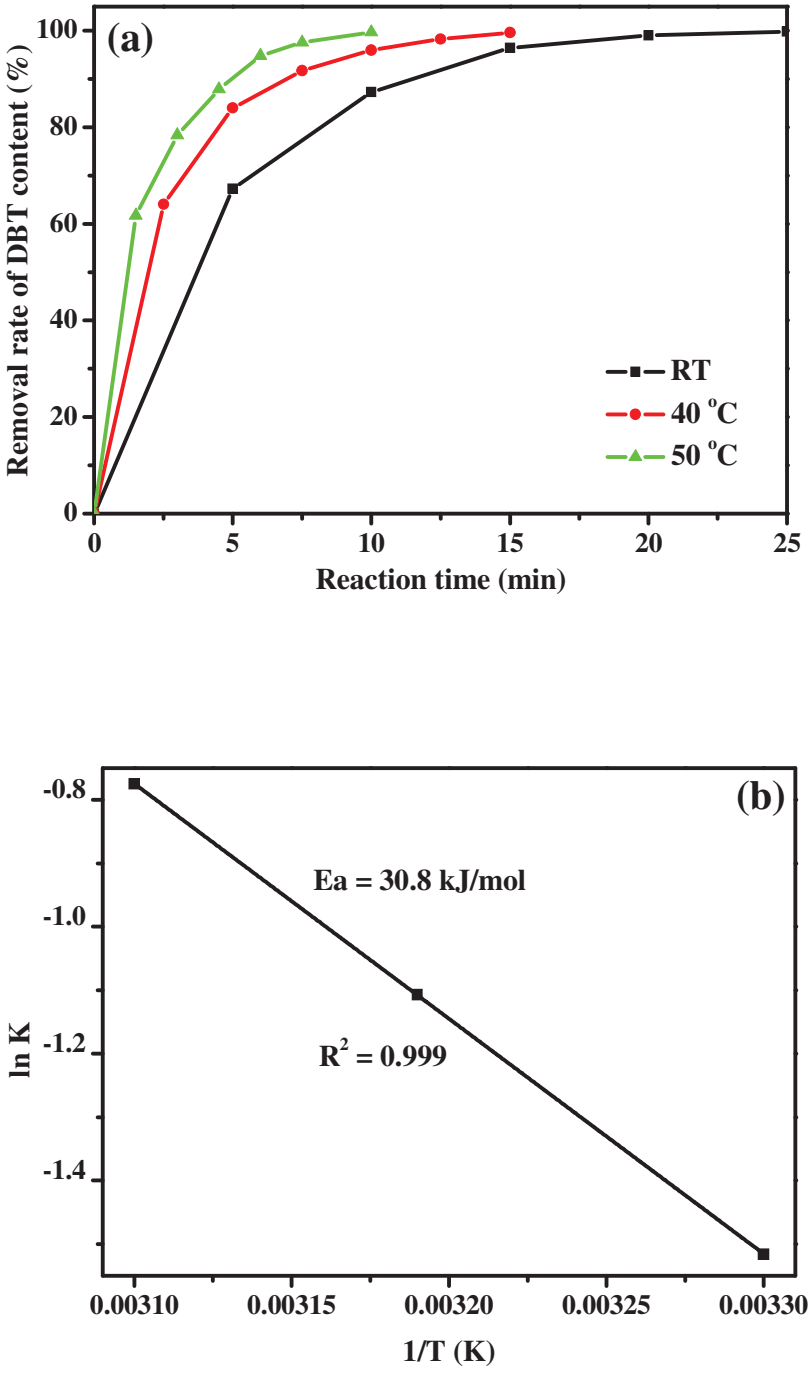
(a)
Removal rate of DBT content (%)
Reaction time (min)
RT
40 °C
50 °C
(b)
ln K
1/T (K)
Ea = 30.8 kJ/mol
R2 = 0.999

Figure 9

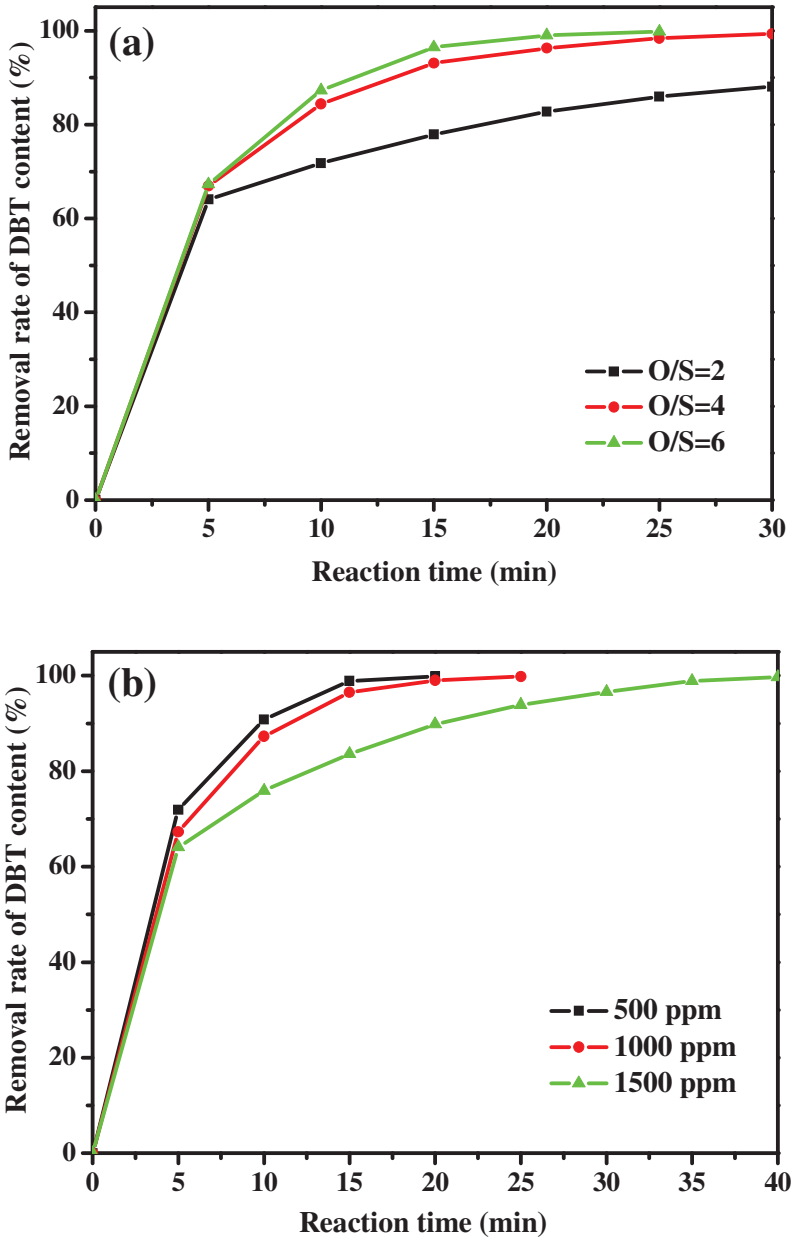
(a)
Removal rate of DBT content (%)
Reaction time (min)
O/S=2
O/S=4
O/S=6
(b)
Removal rate of DBT content (%)
Reaction time (min)
500 ppm
1000 ppm
1500 ppm

Figure 10

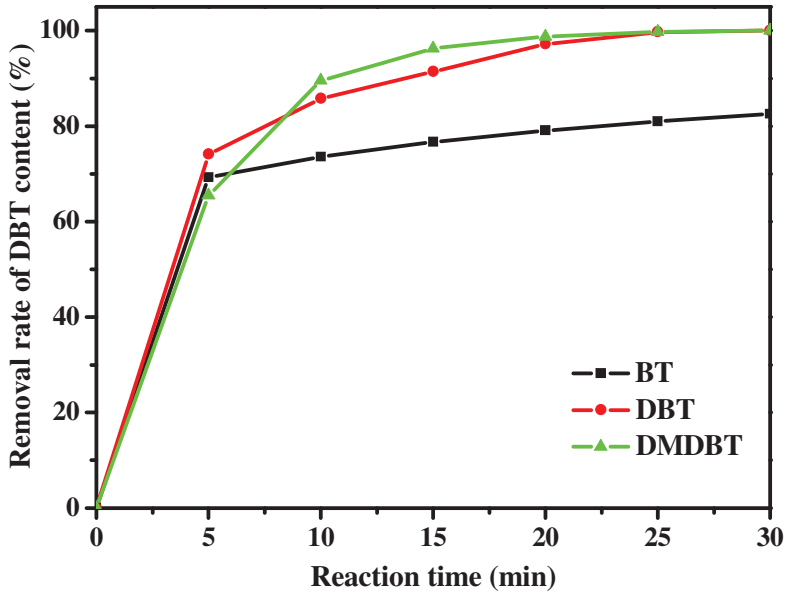
Removal rate of DBT content (%)
100
80
60
40
20
0
0
5
10
15
20
25
30
Reaction time (min)
BT
DBT
DMDBT

Figure 11

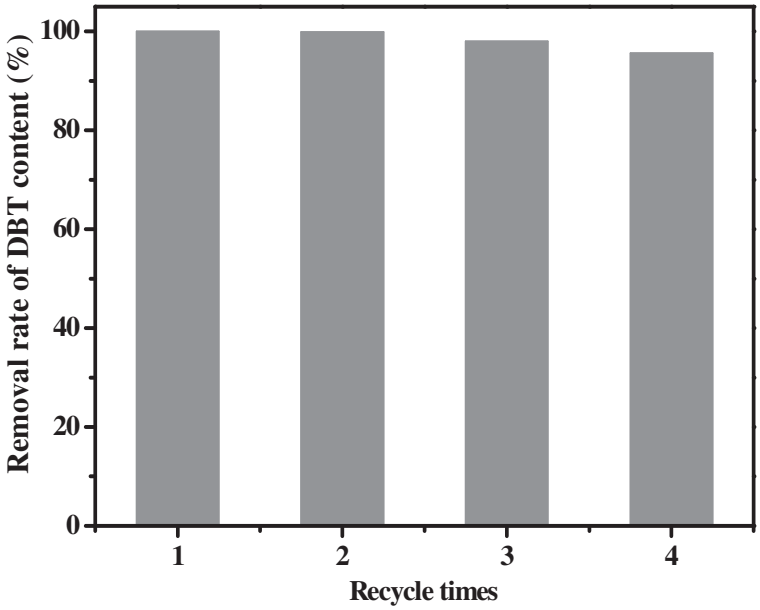
Removal rate of DBT content (%)
100
80
60
40
20
0
1
2
3
4
Recycle times

Figure 12

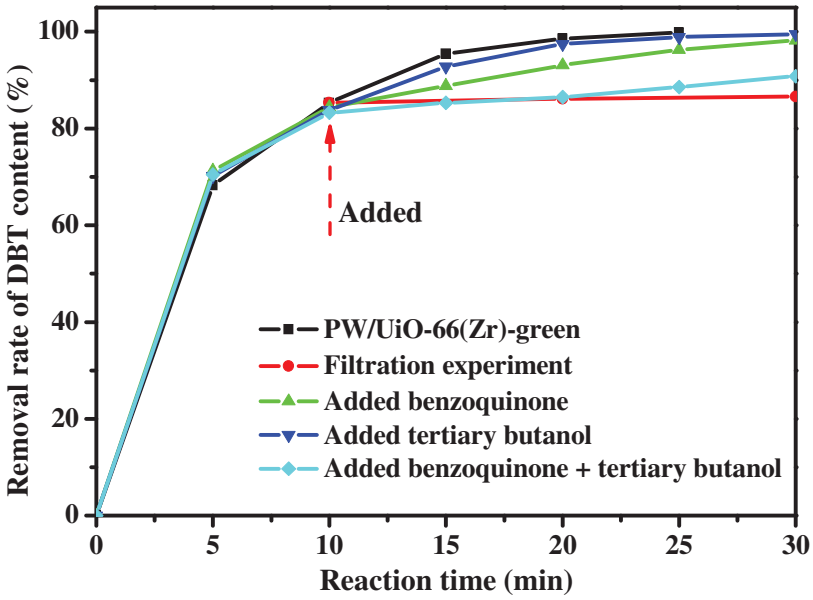
Removal rate of DBT content (%)
Reaction time (min)
Added
PW/UiO-66(Zr)-green
Filtration experiment
Added benzoquinone
Added tertiary butanol
Added benzoquinone + tertiary butanol

Figure 13

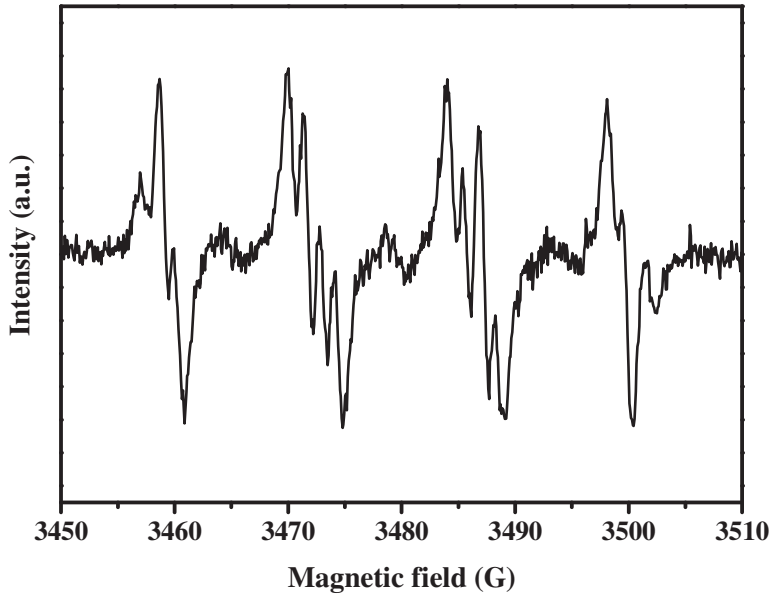
Intensity (a.u.)
3450
3460
3470
3480
3490
3500
3510
Magnetic field (G)

Figure 14